

Claremont Colleges

Scholarship @ Claremont

Scripps Senior Theses


Scripps Student Scholarship

2023

Computational Investigation of the Ionization Potential of Lead Sulfide Quantum Dots

Jessica Beyer

Follow this and additional works at: https://scholarship.claremont.edu/scripps_theses

 Part of the [Computational Chemistry Commons](#), [Inorganic Chemistry Commons](#), [Materials Chemistry Commons](#), [Other Mathematics Commons](#), and the [Physical Chemistry Commons](#)

Recommended Citation

Beyer, Jessica, "Computational Investigation of the Ionization Potential of Lead Sulfide Quantum Dots" (2023). *Scripps Senior Theses*. 2156.
https://scholarship.claremont.edu/scripps_theses/2156

This Open Access Senior Thesis is brought to you for free and open access by the Scripps Student Scholarship at Scholarship @ Claremont. It has been accepted for inclusion in Scripps Senior Theses by an authorized administrator of Scholarship @ Claremont. For more information, please contact scholarship@cuc.claremont.edu.

Computational Investigation of the Ionization Potential of Lead Sulfide Quantum Dots

A Thesis Presented

by

Jessica Beyer

To the Keck Science Department

of

Claremont McKenna, Scripps, and Pitzer Colleges

In Partial Fulfillment of

The Degree of Bachelor of Arts

Senior Thesis in Chemistry

December 10, 2022

Table of Contents

1. Abstract.....	1
2. Motivation and Challenges.....	2
3. Introduction.....	4
3.1 Quantum Dots	4
3.2 Ionization Potential.....	8
3.3 Stratified Stochastic Enumeration of Molecular Orbitals Method.....	8
3.4 Quantum Dot-Ligand Interaction	11
3.5 Core Distortion Due to Ligand Addition	12
4. Materials and Methods	13
4.1 Hydrogen Atom.....	13
4.2 Hartree-Fock	14
4.3 Ionization Potential.....	15
4.4 Quantum Mechanics/Molecular Mechanics	16
4.5 Math Background	17
4.5.1 Monte Carlo Numerical Integration.....	17
4.5.2 Stratified Stochastic Enumeration of Molecular Orbitals Method	20
(SSE-MO).....	20
4.6 Materials for Chemical Systems Studied.....	22
5. Results and Discussion	24

5.1	SSE-MO Verification.....	24
5.2	Timing Results.....	25
5.3	Effect of Nanoparticle Size on Ionization Potential.....	26
5.4	Monodentate Ligands	27
5.4.1	Pb ₄ S ₄ Ligated Systems	27
5.4.2	IP of Ligands Alone.....	28
5.4.3	Ligation Impact on Pb ₄ S ₄	29
5.4.4	Pb ₄₄ S ₄₄ - Ligated System	30
5.5	Bridged Ligands	30
5.6	Chelating Ligands	31
5.7	Future directions	34
6.	<i>Conclusion</i>	36
7.	<i>References</i>	38

Tables

Table 1. Estimated Computation Time of QD IP Using Traditional Quantum Chemical Methods	10
Table 2. Estimated Computation Time of QD-Ligated System IP Using Traditional Quantum Chemical Methods	10
Table 3. SSE-MO performance test for systems with known IP values	25
Table 4. Comparison of computational time for bare core QDs	25
Table 5. Comparison of computational time for Pb ₄ S ₄ -ligated systems	25
Table 6. Effect of QD Size on IP	26
Table 7. IP of Pb ₄ S ₄ – ligated systems	27
Table 8. IPs of the carbonyl-based ligands without the Pb ₄ S ₄ quantum dot	28
Table 9. Impact of ligation on Pb ₄ S ₄ bare cores	29
Table 10. Non-bridged calculated IPs for the Pb ₄₄ S ₄₄ system.....	30
Table 11. Non-bridged calculated IPs for the Pb ₄₄ S ₄₄ system.....	31

Figures

Figure 1. Demonstration of how the density of states changes with the dimensionality of the system. In this work the quantum dot density of states is being analyzed.....	4
Figure 2. A schematic detailing how bridged, monodentate, and chelating ligands interact with the lead atom in the lead sulfide systems.....	12
Figure 3. Random points are chosen within the area A and the integral of the function is the estimated area of A times the fraction of random points in the shaded region.....	18
Figure 4. Demonstrates how as the number of points increases, the more accurate the integral calculations are.....	19
Figure 5. The dots represent random chosen values across $f(x)$. The area shaded is the value being calculated by integration.	19
Figure 6. Demonstration of stratified sampling. Region A only needs one point, where region B needs lots of points because there is a larger variance in the function.	21
Figure 7. From left to right: Pb_4S_4 bare core, $\text{Pb}_{44}\text{S}_{44}$ bare core, and $\text{Pb}_{140}\text{S}_{140}$ bare core. The lead atoms are grey and sulfur atoms are yellow. These structures are graphically depicted in Avogadro; however, the $\text{Pb}_{44}\text{S}_{44}$, and $\text{Pb}_{140}\text{S}_{140}$ structures used in SSE-MO were created in crystal maker. The $\text{Pb}_{28}\text{S}_{28}$ is not included in this picture, but it additionally had bare core calculations run on it....	22
Figure 8. The five carbonyl-based ligands analyzed with Pb_4S_4	23
Figure 9. Demonstration of the IP relationship between the monodentate and bridged ligands on the $\text{Pb}_{44}\text{S}_{44}$ system. The orange line on the top represents the bridged ligands and the blue, lower line signifies the non-bridged ligands.	Error! Bookmark not defined.

Acknowledgements

Writing a senior thesis has been the most daunting task I have ever tackled. It has been a challenging, but extremely rewarding experience that I could not have done without my numerous support systems. I first want to thank Dr. Arindam Chakraborty at Syracuse University for giving me the opportunity to join his research group through the experience for undergraduates (REU) program in summer of 2021. Since then, he has continued to support my undergraduate research experience and help me in every possible way. Dr. Chakraborty amazes me on a daily basis with his ability to make complex topics simple, I am extremely grateful for the opportunity to work with him and for his constant support throughout this semester. I additionally wish to thank Nicole Spanedda for her patience and guidance over the past year and half. She has taught me everything I know about this research. Nicole is always able to meet and answer any questions I have, while showing up to every meeting full of thesis edits, helping my thesis reach the point that it is at today. Thank you so much to Nicole and Dr. Chakraborty for their time, patience, and guidance throughout this project. I can call myself a published author who has written a full senior thesis, which would not have been possible without these individuals and the opportunities they have provided me with. The REU portion of this research was supported under the National Science Foundation-iREU program grant CHE-1950802. The rest of this research was supported by the National Science Foundation under grant numbers CHE-2102437, CHE-1950802, ACI-1341006, and ACI-1541396. This research additionally would not have been possible without the computational resources provided by Syracuse University.

I wish to thank my supporting faculty at Keck Science. The Keck Science professors have given me more support throughout my four years than I ever could have imagined. I would like to

especially thank my two thesis readers, Professor Bethany Caulkins and Professor Joel Mackey. Professor Caulkins gave me constant feedback and reassurance that I was going to finish my thesis throughout the semester, always having an open door for questions. She was additionally an amazing professor, and I could not be more grateful for the relationship that we have formed. Professor Mackey took time every Friday to meet with the chemistry thesis students and support us in any way he could. His computational chemistry background was invaluable when helping me make edits to my thesis.

Finally, thank you to my peers, friends, teammates, and coach for their constant support. I appreciate my peers who were writing thesis at the same time because I was not doing this task alone. A special thanks to Maren Summers for giving me edits throughout the semester. My friends, teammates, and coach always gave me the extra reassurance I needed. The support systems interlaced throughout Keck Science, with the additional resources of Syracuse University have been unmatched. I never thought I would actually be able to produce a thesis I was proud of, and I have proved myself wrong thanks to those surrounding me throughout this process.

1. Abstract

The purpose of this work was to determine the impact of quantum dot size on ionization potential and to determine how the presence of carbonyl-based ligands affect the ionization potential of lead sulfide quantum dot systems. Ionization potential (IP) is defined as the energy required to remove an electron from an atom, molecule, or material. IP helps scientists determine how reactive the material of interest is, which is crucial information when manufacturing nanomaterials. Accurate quantum chemical calculations of ionization potential are challenging due to the computational cost associated with the numerical solution of the Dyson equation. In this work, the stratified stochastic enumeration of molecular orbitals method (SSE-MO) was used to address this challenge. IP was calculated using the SSE-MO method, a computational chemistry method that utilizes a combination of stratified sampling and stochastic enumeration to obtain IPs in an efficient and accurate manner. This method's accuracy was confirmed on systems with known literature values before utilizing it to calculate the IPs of lead sulfide quantum dots. SSE-MO was used to calculate the ionization potentials of different sized lead sulfide (PbS) bare quantum dots, Pb_4S_4 and $\text{Pb}_{44}\text{S}_{44}$ monodentate (non-bridged) ligated systems, $\text{Pb}_{44}\text{S}_{44}$ bridged ligated systems, and $\text{Pb}_{44}\text{S}_{44}$ chelated ligated systems. The results obtained provide insight into the impact of quantum dot size and the presence of ligands on ionization potentials of PbS quantum dot systems, but further testing must be performed to gain more definitive information on the relationship between IP, quantum dot size, and ligand presence.

2. Motivation and Challenges

Studies show that 68 percent of people between the ages of 18 to 29 and 87 percent of individuals 60 and older check the weather on a daily basis.¹ Standard United States households have the news on a couple of times of week for the sole purpose of seeing the weather forecast. These forecasts are predictions that meteorologists have made based on observational data collected through weather satellites and other instruments, which is then put into different types of forecast models.² Meteorologists combine the outcome of these models with past weather models to provide a forecast to the general public. The forecasts are never perfect; however, they give people an idea of what to be prepared for in terms of weather on a given day. Weather forecasts can be thought of as a prediction of future conditions.

Similarly, science can help predict the future. It may not always be 100% accurate and there are bumps along the way, but one way science tries to forecast future outcomes is with computational models that help identify the materials needed to construct different compounds. This saves time and money while keeping individuals working in the lab safer. This paper focuses on lead sulfide (PbS) quantum dots and the ionization potential associated with different-sized PbS systems. Bare and ligated PbS quantum dots were studied, where a ligand is an ion or molecule that binds to a central atom to form a coordination complex.³ Quantum dots are frequently used in technology, specifically televisions and LED lights, due to their ability to control color output and brightness based on their size.

The overall goal of this work is to predict the ionization potential of nanomaterials utilizing computational methods. Similar to the models used in weather forecasting, computational

chemistry can form a connection into virtual reality. A variety of instruments and programs have been created that can perform virtual chemistry while producing insight into reality, which makes this area of science unique. This aspect allows for the interactions in chemical systems to be observed in much greater detail than they could be otherwise.

A new computational chemistry method called the stratified stochastic enumeration of molecular orbitals (SSE-MO) has been developed to be utilized throughout many aspects of quantum chemistry. This method allows for the timely and accurate calculation of ionization potentials (IPs) of large chemical systems. Ionization potential is defined as the energy required to remove an electron from an atom, molecule, or material in the gas phase.



Calculating the IP of larger systems has always been challenging due to the calculation time required. One method to calculate IP is through solving the Dyson equation, which has an iterative solution. In computational work as the size of system increases, the computation time dramatically increases. Traditional computational methods do not produce results in a reasonable amount of time for large chemical systems. Therefore, the development of the SSE-MO method enables the determination of IPs by solving the Dyson equation, even for large chemical systems, such as semiconductor nanoparticles. This work focusses on utilizing SSE-MO to predict the ionization potentials of different sized lead sulfide (PbS) systems with different orientations of ligand attachment and types of ligands, an aspect that has not been previously investigated computationally.⁴ These methods will help scientists identify nanomaterials for technological applications in a more efficient and cost-effective manner.

3. Introduction

3.1 Quantum Dots

Quantum dots are synthesized, nanoscale, semi-conducting crystals that transport electrons. Their highly compact structure makes them one of the most unique materials to work with in the present day. Quantum dots come in many shapes, sizes, compositions, and structures; some are hollow while others are solid.⁵ Quantum confinement is a natural phenomenon seen within quantum dots.

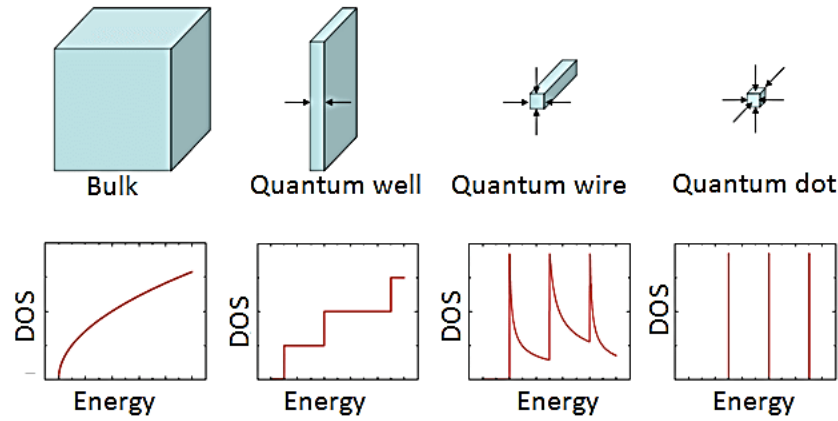


Figure 1. Demonstration of how the density of states changes with the dimensionality of the system. In this work the quantum dot density of states is being analyzed. Obtained from Jayawardhana et. al (2017).⁷

This effect can be observed when there is a decrease in the density of states with decreasing quantum dot size. The density of states helps determine many crucial characteristics of quantum dots such as the mechanical, optical, and electric properties of semiconductor nanomaterials. The density of states exponentially decreases as the energy level of quantum dots increase.⁶

The density of states depends on the dimensionality of the system being analyzed as shown in **Figure 1**. In this work this effect is seen within quantum dots. When increasing the size of a quantum dot, the density of states increases meaning that there are more energy levels in the quantum dot system.⁷ The quantum confinement effect becomes important when nanocrystals

approach the Broglie wavelength of electrons, $\lambda_e = \frac{h}{\sqrt{2\pi mk_B T}}$, also known as the thermal de Broglie wavelength. In this equation m signifies the mass of an electron.⁸ These characteristics determine the properties of each individual quantum dot. This idea of the quantum confinement effect leads to a sharper density of states in quantum dots than in bulk structures, as shown in **Figure 1**.^{9, 10, 11}

Quantum dots have numerous applications due to their unique characteristics. As a result of several controllable properties, quantum dots can emit specific colors of light, making them useful for optical applications. A quantum dot with a 6-nm diameter will emit red light, whereas a quantum dot with a 2-nm diameter will emit blue light, and there are sizes in between that can emit the unique colors between these two.⁵ This allows for color output in technology to be easily governed. Quantum dots are becoming extremely popular in television development as they allow for peak brightness to be regulated, resulting in higher resolution and more color control. For these same reasons quantum dots are utilized in LED lights.

Quantum dots are additionally used within photovoltaics as light emitting diodes where they provide a boost of energy conversion efficiency.¹² PbS quantum dots, specifically, are the building blocks for optoelectronic devices, which are used to detect or emit electromagnetic radiation.¹³ Optical emission spectroscopy is when an electrical energy is applied to an atom and a discharge plasma is created. These excited atoms and ions create a unique emission spectrum that is specific to each element. Therefore, this form of spectroscopy allows for the different elements within a sample to be identified, with a more intense spectra signifying a higher concentration of that sample in the atom.¹⁴ This method is extremely useful to determine the composition of samples.

Furthermore, PbS quantum dots allow for optical emission tunable in the near-infrared wavelength. This means that PbS dots allow for different elements that can only be seen in the near-infrared wavelength within optical emission spectroscopy to be observed and determined for the sample composition. Finally, the efficiency in which a ligand binds to the surface of a quantum dot has been shown to influence polydispersity, quantum yield, and photostability of a nanocrystal, all crucial properties when manufacturing nanomaterials.¹⁵

The quantum dot properties discussed above are extremely useful in different forms of biomedical nanotechnology. Quantum dots aid in diagnosing cancer and other life-threatening diseases due to their small size and optical properties, which is useful in medical imaging. Semiconducting quantum dots are used in biomedical imaging to enable diagnostics for single molecule probes, and in real-time imaging of tumors due to their unique size and shape.¹⁶ Furthermore, the quantum confinement effect is demonstrated when utilizing quantum dots for *in vivo* imaging in biological systems.⁹⁻¹¹ Quantum dots allow images to be recorded over longer periods of time than fluorescent dyes or proteins due to their resistance to photobleaching. For example, chemically modified peptides and biomolecules have been shown to absorb spontaneously on the surface of different quantum dots. Quantum dots coated with these absorbed peptides have been used for *in vivo* imaging to locate cells with specific surface proteins or different types of vasculatures in tumors and organs, the color emission makes them easy to locate. In addition, there have been successful use of *in vivo* tumor imaging by quantum dots in mice, a biological system.¹⁷ Furthermore, quantum dots are used in drug delivery as fluorophores, instead of dyes, due to the fact that they have little degradation over time and are brighter than dyes. They are also preferred

over dyes due to the size dependence of their optical properties, which enables access to the entire color spectrum.¹⁸

There are many different types of quantum dots, but this work focuses on lead sulfide (PbS) quantum dots. PbS quantum dots were chosen for many reasons, primarily due to their low cost. Cadmium sulfide (CdS) quantum dots are also popular in research settings, but isolated PbS quantum dots have a microsecond fluorescence lifetime two orders of magnitude longer than that of isolated CdS. This means that the emitted colors from the dot last longer for PbS than for the CdS quantum dots.¹⁹ PbS quantum dots show a strong size dependence in that their electron affinity and IP are strongly affected due to quantum confinement, the same phenomenon that causes different-sized dots to be specific colors.¹⁹ This means that the size of the quantum dot has a large impact on electron affinity, the change in energy when an electron is added to form an anion, and IP.²⁰ Lastly, PbS quantum dots are utilized within solar cells since their energy can be made to overlap with, and therefore efficiently use, the solar spectrum through the ability to control their size.¹⁹ Lead sulfide quantum dots are unique compared to other types of quantum dots in that they produce more than 100% of solar cell efficiency due to multiexciton generation.²¹ Therefore, PbS quantum dots convert sunlight into more energy than they originally absorbed using photovoltaics. This is extremely unique and beneficial for solar energy applications.

In addition, PbS quantum dots have a high bulk excitation Bohr radius and narrow bandgap. This combination allows for the quantum confinement effect to occur with relatively large crystallites, which is difficult to do with most materials. These properties make them useful for doped glass fabrication.²² In addition, PbS quantum dots are utilized in the detection of x-ray radiation. The

high density produced from quantum confinement and quantum dot's high atomic number enable this detection.²³ Having a more broad range of knowledge on PbS quantum dots is beneficial due to their wide variety of applications.

3.2 Ionization Potential

Ionization potential (IP) is the energy required to remove an electron from an atom, molecule, or material in the gas phase. The smaller the IP, the less energy required to remove an electron from the molecule, and therefore, the more reactive the molecule of interest is. IP is most commonly known by its periodic trend: it increases across a period and decreases down a group. This concept becomes crucial when performing reactions because it allows for the reactivity of a molecule to be estimated. Knowing the reactivity of a molecule saves time, money, materials in the lab, and helps predict the strength of a chemical bond, which is an indicator of reactivity.²⁴ IP has many applications within science. For example, electron transfer reactions utilized by photovoltaics are the most common use of IP.²⁵ The process of ionization additionally generates the positively charged fragments analyzed in mass spectrometry.²⁶

3.3 Stratified Stochastic Enumeration of Molecular Orbitals Method

The stratified stochastic enumeration of molecular orbitals (SSE-MO) method is a new, recently developed, peer-reviewed, and published computational chemistry method that produces fast and accurate predictions of IPs for chemical systems that are computationally impractical to obtain otherwise.⁴ Computational chemistry comes with challenges and advantages. Scientists always face the dual challenges of time and money constraints. In this work, time was a challenge as traditional computational softwares do not allow for the IP of larger systems to be calculated in a

reasonable amount of time. The equation utilized to calculate IP in this work is called the Dyson equation, which is defined as follows.

$$\Sigma(\omega) + \omega^0 = \omega \quad (\text{Equation 2})$$

In this equation ω represents ionization potential and $\Sigma(\omega)$ is the self-energy term. In this work, the self-energy term is approximated as

$$\Sigma_{ii} \approx \Sigma_{ii}^{(2)}(\omega) = \frac{1}{2} \sum_{jab} \frac{\langle ij | r_{12}^{-1} | ab \rangle_A \langle ab | r_{12}^{-1} | ij \rangle_A}{\omega + \epsilon_j - \epsilon_a - \epsilon_b} + \frac{1}{2} \sum_{jak} \frac{\langle ia | r_{12}^{-1} | jk \rangle_A \langle jk | r_{12}^{-1} | ia \rangle_A}{\omega + \epsilon_a - \epsilon_j - \epsilon_k}. \quad (\text{Equation 3})$$

The indices i, j , and k indicate occupied spin orbitals, while a and b indicate virtual spin orbitals. The main point to understand from these equations is that the ω term, or ionization potential, appears on both sides of the equation (**Equation 3**). Therefore, the Dyson equation must be solved iteratively. For systems with a large number of orbitals, solving the Dyson equation becomes impractical due to the calculation time required. In the self-energy term, the calculation time for $\sum_{jab}^N \approx N^3$ and the calculation time for $\langle ij | r_{12}^{-1} | ab \rangle \approx N^5$. Therefore, the total computation time becomes $N^3 + N^5$, where N represents the number of orbitals in the system. This means that as the size of the chemical system increases, the computational calculation time required to determine IP dramatically increases. In larger systems such as $\text{Pb}_{140}\text{S}_{140}$ it is computationally impractical to find the IP using traditional methods as it would take almost four years to calculate as shown in **Table 1** and **Table 2**. Therefore, a new efficient method such as SSE-MO must be used to calculate IP.

Table 1. Estimated Computation Time of QD IP Using Traditional Quantum Chemical Methods

Quantum Dots	Expected Computation Time
Pb ₄ S ₄	1.07 hours
Pb ₂₈ S ₂₈	15.27 days
Pb ₄₄ S ₄₄	59.24 days
Pb ₁₄₀ S ₁₄₀	1438.24 days

Table 2. Estimated Computation Time of QD-Ligated System IP Using Traditional Quantum Chemical Methods

Quantum Dots	Expected Computation Time
Pb ₄ S ₄ – Ligand 1	1.07 days
Pb ₄ S ₄ – Ligand 2	2.26 days
Pb ₄ S ₄ – Ligand 3	4.09 days
Pb ₄ S ₄ – Ligand 4	9.25 days
Pb ₄ S ₄ – Ligand 5	10.28 days

This work focuses on nanomaterials, which are difficult to make in a lab due to the high pressure and temperature necessary to do so.²⁷ Therefore, computational methods reduce the risk that comes with these conditions and makes analyzing nanomaterials much safer. The pressure and temperature used in producing nanomaterials highly differ when making a small amount versus producing them in bulk, which has a large impact on manufacturing.²⁸ Computation helps predict which materials should be used in the final product once it goes into manufacturing which saves time, money, and materials.⁴

3.4 Quantum Dot-Ligand Interaction

This study analyzes the effect of the addition of a variety of carbonyl-based ligands on IP. Three different forms of ligands were attached to the lead atoms analyzed: monodentate ligands, bridged ligands, and chelating ligands. The monodentate ligands investigated in this study are non-bridged and non-chelating carbonyl-based ligands that differ by the number of $-CH_2$ groups they contain. These ligands were chosen because they have been used in previous experiments, which enables a slight prediction of their behavior.²⁹ In addition, they have not been used in previous experiments that involve IP, meaning there is room for new discoveries with these ligands.

Due to the small size of Pb_4S_4 , only monodentate ligands were attached to this quantum dot. For Pb_4S_4 , one carbonyl-based ligand was attached to each of the four lead atoms by a single bond between an oxygen atom of the ligand and the lead atom of the quantum dot, completely saturating the system.

Bridged ligands are ligands that form a bridge between two atoms (**Figure 2**), in this case two lead atoms.³⁰ These ligands are normally organic compounds that bind to metals and help spatially orient the metal atoms that they bridge.³¹ In this instance, OOH ligands were used on the $Pb_{44}S_{44}$ quantum dot system. Each oxygen was connected to its own lead atom in the system, with the oxygens on the same ligand attached to neighboring lead atoms.

Chelating ligands allow both oxygens from the same carbonyl-based ligand to connect to the same lead atom, **Figure 2**.³⁰ This type of ligand bonds metals by having each oxygen donate a pair of their electrons to the metal, which creates a bond between the ligand and the metal.³² Once again, OOH ligands were used with the $\text{Pb}_{44}\text{S}_{44}$ system.

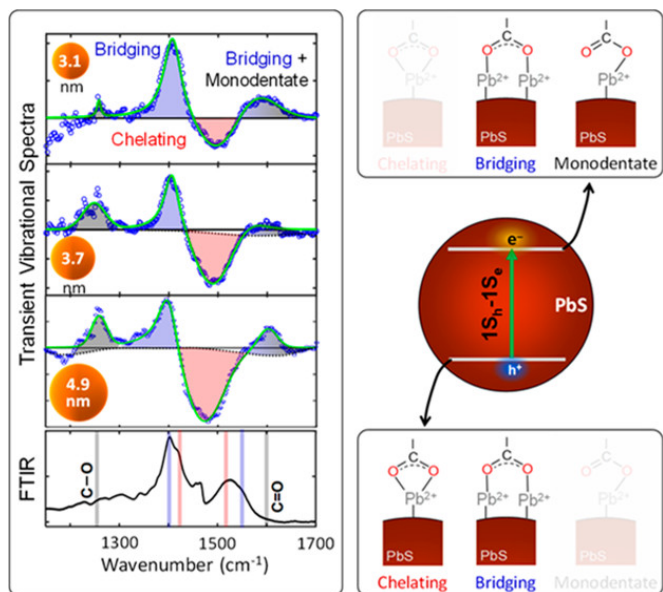


Figure 2. A schematic detailing how bridged, monodentate, and chelating ligands interact with the lead atom in the lead sulfide systems. Obtained from Kennehan et. al 2020.³⁰

3.5 Core Distortion Due to Ligand Addition

When ligands are attached to a quantum dot, the core geometry of the quantum dot changes. In this study, it was determined whether the presence of ligands on the Pb_4S_4 core had an impact on the IP of the bare core. This was done by first adding ligands to the Pb_4S_4 dot and then performing a geometry optimization on the ligated dot. Next, the ligands were stripped from the dot, leaving behind a distorted bare Pb_4S_4 core. This was followed by SSE-MO calculations to find the IPs of the distorted bare Pb_4S_4 cores.

4. Materials and Methods

4.1 Hydrogen Atom

The Schrödinger equation calculates the energy of a system utilizing a Hamiltonian operation on the given system. The time-independent Schrödinger equation (TISE) is defined as

$$\hat{H}\Psi = E\Psi, \quad (\text{Equation 4})$$

where \hat{H} is the Hamiltonian operator for the system, Ψ represents the wave function of the system, and E is the energy of the system.

In chemistry the hydrogen atom is of large interest as it serves as an extremely simplified prototype for more complex atoms, molecules, and systems. For the hydrogen atom, the Schrödinger equation can be solved exactly, which is not the case for any other system because the systems are too complex to solve exactly, meaning solutions to these systems are approximations. In this case, the hydrogen atom model contains a proton fixed at the origin and an electron interacting with the proton through a Coulombic potential. This model has a spherical geometry, meaning that a spherical coordinate system where the proton sits at the origin is used to visualize the system. The Hamiltonian operator for a hydrogen atom is defined as

$$\hat{H} = -\frac{\hbar}{2m_e}\nabla^2 - \frac{e^2}{4\pi\epsilon_0 r}, \quad (\text{Equation 5})$$

where ∇^2 is the Laplacian operator in spherical coordinates. When plugging the system's Hamiltonian into the Schrödinger equation an extremely complicated equation is produced. This is not possible to solve exactly for any system containing more than one electron, meaning that computational methods are required to approximate a solution for multi-electron systems.

The principal quantum number (n) depends on the state of the atom and can be any integer that is greater than zero. For example, if the first energy level is being analyzed, then n would equal 1.

The energy of a hydrogen atom depends only upon the principal quantum number, as shown.

$$E_n = -\frac{Rh}{n^2} = -\frac{e^2}{8\pi\epsilon_0 a_0 n^2} \quad (\text{Equation 6})$$

This is the amount of energy required to knock off a hydrogen atom from a system or molecule.³³

4.2 Hartree-Fock

The Hartree-Fock method is the conceptual basis for molecular orbital theory and the foundation of numerous orbital theories within chemistry. Hartree-Fock calculations produce approximate results for molecular orbital calculations; these results are exact for the hydrogen atom and strong estimates for other systems as exact solutions to the Schrödinger equation are not possible to obtain in larger systems. This method was developed to solve the electronic Schrödinger equation; solving this equation provides the potential energy surface and valuable information about the wavefunction being analyzed.³⁴

The Hartree-Fock method can be define as

$$\hat{F}_i \phi_i = \epsilon_i \phi_i, \quad (\text{Equation 7})$$

where \hat{F}_i is the Fock operator, similar to the Hamiltonian operator, ϕ_i are molecular orbitals, and

the orbital energies are denoted as ϵ_i . $\hat{F}_i \phi_i = \epsilon_i \phi_i$, (Equation 7)

must be solved in a self-consistent manner because ϕ_i appears on both sides, meaning \hat{F}_i depends on ϕ_i . Therefore, this equation must be solved multiple times before a solution is reached, a self-

consistent approach. $\hat{F}_i \phi_i = \epsilon_i \phi_i$, (Equation 7 is solved when

the right-hand side of the equation is numerically equal to the left-hand side of the equation within some error tolerance, typically 1×10^{-5} Hartrees. Computer programs are used to solve for these self-consistent orbitals, known as the Hartree-Fock orbitals. When the error tolerance is reached the calculations are considered converged and the program will terminate. In addition, these computer programs solve for ϵ_i , the eigenvalues from $\mathbf{F}i \cdot \phi_i = \epsilon_i \phi_i$, (Equation 7, known as the orbital energies.³³

The Hartree-Fock method is widely used throughout quantum chemistry and does not provide an exact solution to the Schrödinger equation. The difference between the exact energy and the energy found using the Hartree Fock energy is known as the correlation energy, $E_{corr} = E_{exact} - E_{HF}$

(Equation 8.

$$E_{corr} = E_{exact} - E_{HF} \quad (\text{Equation 8})$$

Post-Hartree-Fock calculations are performed to account for errors that arise from using the Hartree Fock method. E_{exact} cannot be determined with complete accuracy for many electron systems using existing theoretical and computational methods. In a practical setting, E_{exact} is often approximated after obtaining E_{corr} to account for the errors that arise in the Hartree Fock method.

4.3 Ionization Potential

The ionization potential (IP) demonstrates the amount of energy needed to eject an electron from a molecule, which measures how strongly the electron is bound to a molecule. The value obtained for IP depends on the molecular orbital that the electron being analyzed occupies; the lower the energy of the molecular orbital, the more energy required to remove an electron from that orbital.

Koopman's theorem approximates the IP of molecular systems and is defined as

$$IP \approx -\epsilon_1. \quad (\text{Equation 9})$$

This approximation assumes that the same orbitals can be used to calculate the energy of a neutral atom and the energy of a charged atom or ion. According to Koopmans Approximation, $-\epsilon_i$ $F_i \phi_i = \epsilon_i \phi_i$, (Equation 7) is the ionization energy of an electron in the i^{th} orbital.³³ Therefore, Hartree-Fock calculations can calculate the IP of different molecular orbitals by applying Koopmans theorem.

4.4 Quantum Mechanics/Molecular Mechanics

Quantum mechanics/molecular mechanics (QM/MM) are utilized to simulate dynamic chemical processes. When describing quantum mechanical systems, it is crucial to use a quantum mechanical approach, instead of a classical mechanics approach, to accurately depict the system. In molecular mechanics the MM regions utilize partial charges on atoms instead of electrons. Therefore, this method replaces the explicit electrons within the system with partial charges associated with the different atoms. This results in a fewer number atoms in the system, and therefore, decreases the computational cost and complexity of the system. On the Hartree-Fock level, the number of terms (n) in the wavefunction is proportional to n factorial. A singular lead atom has 82 electrons, which has 4.57×10^{122} terms as calculated from $82!$. For two lead atoms there are 164 electrons and 3.29×10^{293} terms. Therefore, adding just one lead atom significantly increases the number of terms in the wavefunction being solved. For $\text{Pb}_{140}\text{S}_{140}$ there are 11,480 electrons solely for the lead atoms, $n!$ for 11,480 returns "infinity" when plugged into a basic calculator. In comparison, when using MM with $\text{Pb}_{140}\text{S}_{140}$, 280 atoms are accounted for instead of more than 11,480 electrons due to the use of partial charges. Overall, decreasing the total number

of terms in the wavefunction significantly decreases the complexity of the system making this method much more efficient. In this work, the ligands added account for the extra electrons if everything is treated quantum mechanically, which greatly reduces the total number of electrons in the system. The QM aspect provides accuracy as quantum mechanics should be used for quantum mechanical systems, and the MM aspect provides speed as it decreases the complexity of the systems analyzed. This is by far the best method to analyze these large systems because it decreases their complexity. There are numerous different aspects of QM/MM, but this work utilizes electrostatic embedding.

For quantum dots, their nonbonding nature allows for a simple treatment of the QM/MM boundary. The quantum dot's interactions can be modeled using a Hamiltonian, and eigenvalues can be obtained from the solution of the following equation.³⁵

$$\left[\frac{-\hbar}{2m} \nabla^2 + v_{ps}(r, R^{dot}) + v_{ext}^{QM/MM}(r, R^{interaction}) \right] \phi_i = \epsilon_i \phi_i \quad (\text{Equation 10})$$

Overall, electrostatic embedding requires more computational effort than other forms of QM/MM, but is extremely useful when analyzing quantum dot interactions.³⁶

4.5 Math Background

4.5.1 Monte Carlo Numerical Integration

4.5.1.1 General Background

Integrals are most simply known as the area under a curve, the curve being the function that is being integrated. Monte Carlo numerical integration is a form of integration that utilizes random

sampling and “averaging” to approximate integrals. This method can be used to estimate the integral of a function f over a one dimensional or multi-dimensional volume of space.

$$\int f dV \approx V \langle f \rangle \pm V \sqrt{\frac{\langle f^2 \rangle - \langle f \rangle^2}{N}} \quad (\text{Equation 11})$$

In the above equation V denotes the volume of space over which the function f is integrated. The plus/minus term in this equation represents one standard deviation error estimate for the calculated integral.

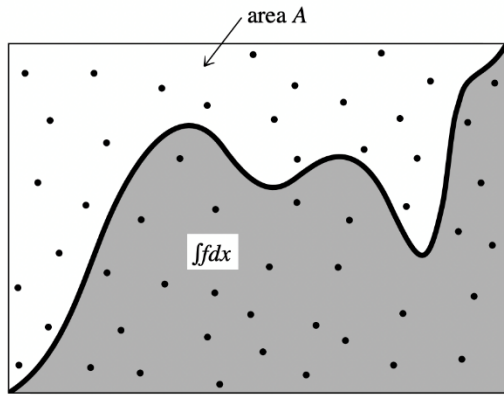


Figure 3 demonstrates how random points are chosen within the entire area of A. The integral of the function $f(x)$ is then estimated as the area of A times the fraction of the random points that fall below the curve of $f(x)$, the shaded region. Randomly distributed points cover the entire area, a random sampling variation.³⁷

Figure 3. Random points are chosen within the area A and the integral of the function is the estimated area of A times the fraction of random points in the shaded region. Obtained from William et al (1986).³⁷

As shown in **Figure 4**, as the number of random sampling points increases, the accuracy of the integral dramatically increases. From this it can be concluded that, the fractional accuracy of Monte Carlo numerical integration can be modeled as a function of the number of points sampled for two different integrands and two separate random points.

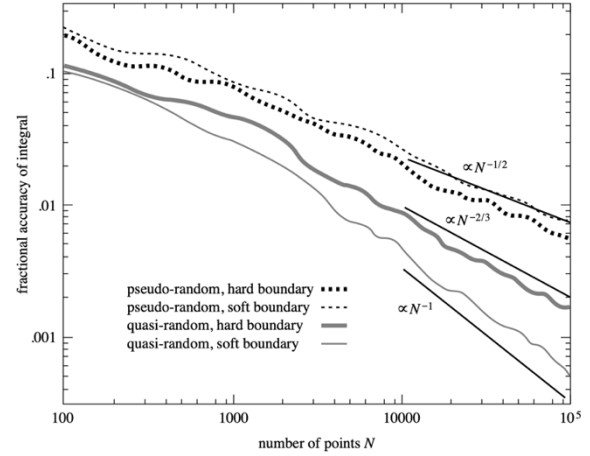


Figure 4. Demonstrates how as the number of points increases, the more accurate the integral calculations are. Obtained from William et al (1986).³⁷

4.5.1.2 Steps for Solving

Monte Carlo numerical integration can be used to solve integrals in the form $\int_a^b f(x)dx$. First, random values of x are chosen at which to evaluate $f(x)$ at. The number of randomly chosen values for x is then recorded to keep track of these values. After choosing N number of values for x , the average value for $f(x)$ is determined by

$$\bar{f} = \frac{1}{N} \sum_{i=1}^N f(x_i). \quad (\text{Equation 12})$$

Finally, \bar{f} is multiplied by the volume of space that function is being integrated over and the integral is solved as shown in **Figure 5**.

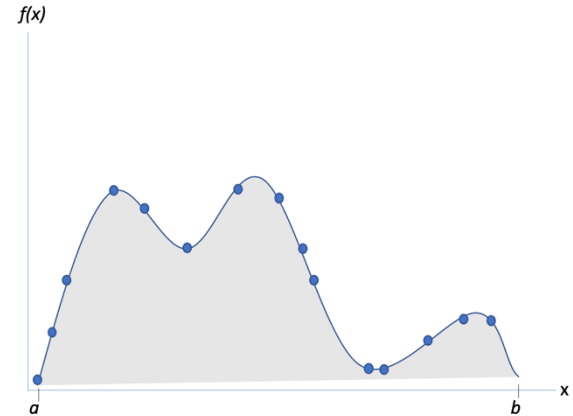


Figure 5. The dots represent random chosen values across $f(x)$. The area shaded is the value being calculated by integration.

4.5.1.3 Advantages

There are numerous advantages of Monte Carlo numerical integration, but there are two principal advantages. First, this form of integration can be used to approximate integrals where the analytical form of the function being integrated is unknown, meaning that only inputs and outputs are required. Second, the error in the approximation for the integral is well defined. The standard deviation (square root of the variance) of the integral being solved is

$$\sigma = \sqrt{\frac{1}{N} \sum_{i=1}^N [f(x_i)]^2 - [\bar{f}]^2}. \quad (\text{Equation 13})$$

This equation demonstrates that the error in the estimate is proportional to $\frac{1}{\sqrt{N}}$. Therefore, the error within this method can be significantly reduced by increasing the number of sampling points. The number of sampling points does not need to increase with the number of dimensions, which is advantageous when numerically solving integrals of higher dimensions.

4.5.2 Stratified Stochastic Enumeration of Molecular Orbitals Method

(SSE-MO)

The recently developed stratified stochastic enumeration of molecular orbitals method (SSE-MO) calculates the IP of different systems. SSE-MO can be used to obtain the self-energy and subsequently correct for the errors within the Koopmans IP.

The SSE-MO method combines the concepts of stochastic enumeration and stratified sampling to obtain IPs in an efficient manner while maintaining accuracy. There are two main components to this method: stochastic enumeration and stratified sampling. Stochastic enumeration performs a summation of a large number of terms stochastically instead of sequentially, which dramatically

increases the efficiency in computing the summation involved in the calculations required to solve

the Dyson equation for IP (ω). $f_{sum} = \sum_{i=1}^{10^{10}} f(i) \approx 10^{10} \times \frac{1}{N_{sample}} \sum_{i \in 1, \dots, 10^{10}}^{N_{sample}} f(i)$

(Equation 14 demonstrates how stochastic enumeration is performed in a mathematical context.

$$f_{sum} = \sum_{i=1}^{10^{10}} f(i) \approx 10^{10} \times \frac{1}{N_{sample}} \sum_{i \in 1, \dots, 10^{10}}^{N_{sample}} f(i) \quad (\text{Equation 14})$$

Stratified sampling divides the sample space of a function into segments. The segments that should be further sampled are determined to increase the accuracy in the estimate of an integral calculated using Monte Carlo numerical integration. More sampling points are allocated to the segments where a greater variance is observed, ultimately increasing the

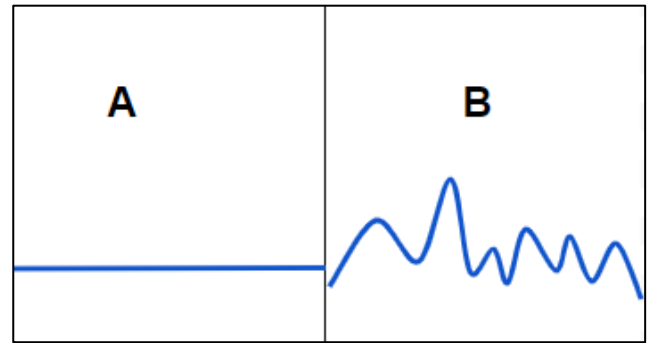


Figure 6. Demonstration of stratified sampling. Region A only needs one point, where region B needs lots of points because there is a larger variance in the function.

accuracy of the integral. In **Figure 6**, the function of interest has little variance or fluctuation in region A. Therefore, only one sampling point is necessary for accurate Monte Carlo integration in this region. Whereas, the function displays a much greater variance in region B, meaning more random sampling points are needed in this region for accurate Monte Carlo Integration. The use of stratified sampling enables efficient sampling while maintaining accuracy in the estimate of the integral from Monte Carlo numerical integration.

In the SSE-MO process, stratified sampling occurs when the code learns about regions of space with high sampling error. Enhanced Monte Carlo numerical integration is performed for these

regions, which improves the efficiency and accuracy with which the integrals needed to solve the Dyson equation are computed. It is important to note that stratified sampling error is less than or equal to simple sampling error. SSE-MO combines stochastic enumeration and stratified sampling to allow for fast and accurate calculations of ionization potential for chemical systems which are computationally impractical to investigate with conventional methods.

4.6 Materials for Chemical Systems Studied

In this project, the SSE-MO calculations were performed on a Syracuse University virtual private network connected to Syracuse servers. This allowed for the use of Syracuse University computing grids, QChem, and Terachem to perform the necessary Hartree-Fock calculations using the LANL2DZ-ECP basis. Terachem was used to perform geometry optimizations on only the Pb_4S_4 bare core and ligated systems.

Avogadro and Crystal Maker were utilized to generate the structures for the PbS systems evaluated in this project. The bare and ligated Pb_4S_4 structures were generated in Avogadro before using

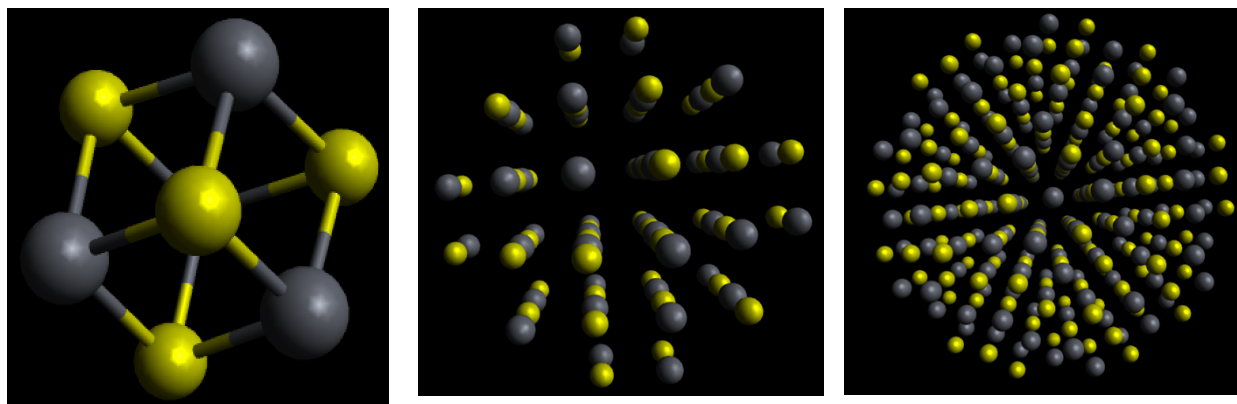


Figure 7. From left to right: Pb_4S_4 bare core, $\text{Pb}_{44}\text{S}_{44}$ bare core, and $\text{Pb}_{140}\text{S}_{140}$ bare core. The lead atoms are grey and sulfur atoms are yellow. These structures are graphically depicted in Avogadro; however, the $\text{Pb}_{44}\text{S}_{44}$, and $\text{Pb}_{140}\text{S}_{140}$ structures used in SSE-MO were created in crystal maker. The $\text{Pb}_{28}\text{S}_{28}$ is not included in this picture, but it additionally had bare core calculations run on it.

Terachem to perform geometry optimizations for these systems. However, this process was not performed on $\text{Pb}_{28}\text{S}_{28}$, $\text{Pb}_{44}\text{S}_{44}$, and $\text{Pb}_{140}\text{S}_{140}$ since their structures were made in Crystal Maker. After obtaining the desired bare core structures, shown in **Figure 7**, Hartree-Fock calculations were performed for both the bare and ligated Pb_4S_4 systems and for the bare $\text{Pb}_{28}\text{S}_{28}$, $\text{Pb}_{44}\text{S}_{44}$, and $\text{Pb}_{140}\text{S}_{140}$ quantum dot systems to obtain the orbitals and orbital energies. SSE-MO was then performed for these systems to determine the effect of quantum dot size on ionization potential. The impact of five different carbonyl-based ligands on the IP of the Pb_4S_4 system was investigated. Each ligand differed by the number of methylene groups it contained, **Figure 8**.

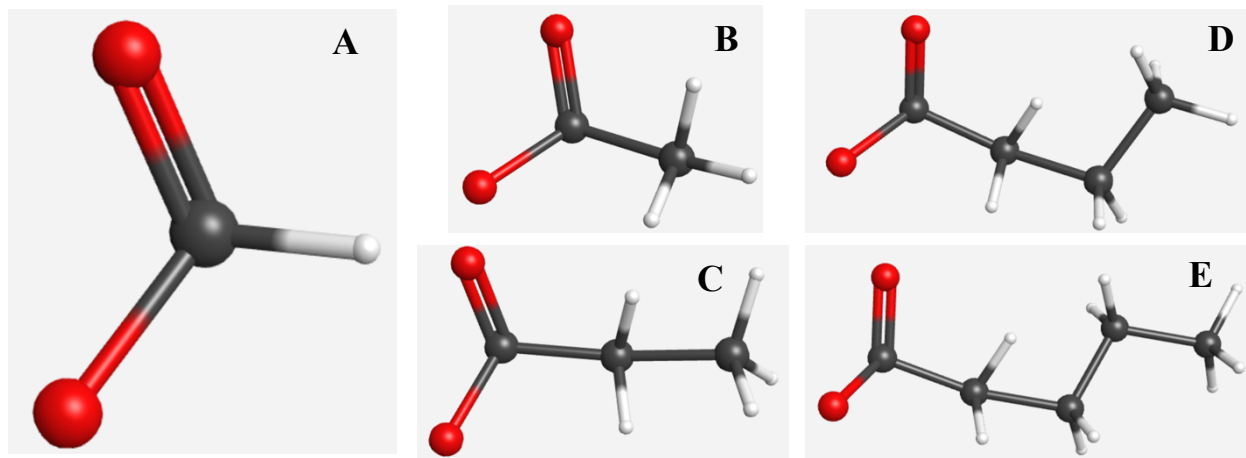


Figure 8. The five carbonyl-based ligands analyzed with Pb_4S_4 .

- A: Ligand 1 – QD-O-CO-H
- B: Ligand 2 – QD-O-CO-CH₃
- C: Ligand 3 – QD-O-CO-CH₂-CH₃
- D: Ligand 4 – QD-O-CO-CH₂-CH₂-CH₃
- E: Ligand 5 – QD-O-CO-CH₂-CH₂-CH₂-CH₃

For the Pb_4S_4 ligated system the ligand being analyzed was attached to each of the four lead atoms on Pb_4S_4 bare core by the oxygen atom single bonded to the alpha carbon, meaning the lead atoms in the core were completely saturated.

In addition, the impact of the bonding patterns of ligand 1 to $\text{Pb}_{44}\text{S}_{44}$ on IP was investigated. Ligand 1 (O-CO-H) was attached to up to six lead atoms depending on the trial for the $\text{Pb}_{44}\text{S}_{44}$ ligated

system. When one ligand was used, it was attached to a random lead atom and the IP calculations were performed. With two ligands, the distance between the previously chosen lead atom and the other lead atoms was calculated. The second ligand was attached to the atom that was furthest away from the original ligand. With three ligands, the distances between the ligated and non-ligated lead atoms were calculated and the third ligand was attached to the lead atom that had the furthest difference from both ligated atoms. This process was repeated with four, five, and six ligands for the $\text{Pb}_{44}\text{S}_{44}$ system. Ligand 1 (O-CO-H) was additionally used for the bridged and chelating $\text{Pb}_{44}\text{S}_{44}$ systems. For the bridged ligand calculations, the two oxygen atoms on ligand 1 were attached to two neighboring lead atoms in the $\text{Pb}_{44}\text{S}_{44}$ system. The number of ligands attached depended on the trial run; there were up to six bridged ligands attached to the system at once. The same ligand configuration structures from the non-bridged calculations were used. The second oxygen atom was attached to a neighboring lead atom, as none of these atoms had ligands attached to them. For the chelating ligand calculations, the two oxygen atoms were attached to the same lead atom of the $\text{Pb}_{44}\text{S}_{44}$ non-bridged ligated systems. Once again, the number of ligands attached to lead atoms depended on the trial. For the chelating bonding pattern, the second oxygen on the ligand was attached to the same lead atom as the first oxygen.

5. Results and Discussion

5.1 SSE-MO Verification

Before testing SSE-MO on systems with unknown IPs, its accuracy had to be confirmed. The accuracy of this method was confirmed by running the SSE-MO code on systems with known literature values for IP: water, methane, and neon.

Table 3. SSE-MO performance test for systems with known IP values

System	SSE-MO IP (eV)	Literature Value (eV)	Standard Dev (eV)
H ₂ O	10.611	10.738	0.081
CH ₄	13.947	13.914	0.033
Ne	21.377	21.134	0.070

As seen in low standard deviations in **Table 3**, IPs obtained for the three systems were close to the known literature values. Therefore, it was concluded that SSE-MO was an accurate method for calculating IP and could be used on other systems with unknown IPs.

5.2 Timing Results

As mentioned, traditional computational methods to calculate ionization potential are extremely inefficient. SSE-MO dramatically decreased the computation time necessary to obtain IP results.

Table 4. Comparison of computational time for bare core QDs

Quantum Dot	Traditional Method	SSE-MO Method
Pb ₄ S ₄	1.07 hours	1.96 minutes
Pb ₂₈ S ₂₈	15.27 days	11.05 minutes
Pb ₄₄ S ₄₄	59.24 days	17.04 minutes
Pb ₁₄₀ S ₁₄₀	1438.24 days	66.93 minutes

Table 5. Comparison of computational time for Pb₄S₄-ligated systems

QD Ligated System	Traditional Method	SSE-MO Method
Pb ₄ S ₄ – Ligand 1	1.07 days	6.39 minutes
Pb ₄ S ₄ – Ligand 2	2.26 days	7.89 minutes

Pb ₄ S ₄ – Ligand 3	4.09 days	9.52 minutes
Pb ₄ S ₄ – Ligand 4	9.25 days	11.06 minutes
Pb ₄ S ₄ – Ligand 5	10.28 days	12.48 minutes

As seen in the data presented in **Table 4** and **Table 5**, SSE-MO allowed for results to be obtained in a reasonable amount of time compared to traditional computational methods. It can be concluded from these computation times that SSE-MO is an efficient method for calculating IP. Combining this with the results from **Table 3**, it can be concluded that SSE-MO is both an accurate and efficient IP calculation method.

5.3 Effect of Nanoparticle Size on Ionization Potential

SSE-MO was utilized to determine how the IP changes as a function of lead sulfide quantum system size.

Table 6. Effect of QD Size on IP

QD System	Dot Diameter (nm)	Calculated IP (eV)
Pb ₄ S ₄	0.2968	7.608 ± 0.028
Pb ₂₈ S ₂₈	0.8904	5.760 ± 0.010
Pb ₄₄ S ₄₄	1.484	6.960 ± 0.008
Pb ₁₄₀ S ₁₄₀	2.078	6.630 ± 0.206

The IP results obtained produced a low error, indicating that the calculation method was accurate.

From

, it can be seen that in general as the size of the quantum dot increases, the calculated IP decreases; however, this trend is not consistent with $\text{Pb}_{28}\text{S}_{28}$. Therefore, larger lead sulfide quantum dot systems are usually less stable than the smaller systems. To further conclude if this trend holds true for the majority of systems, identical calculations must be run on a wider variety of lead sulfide systems.

5.4 Monodentate Ligands

5.4.1 Pb_4S_4 Ligated Systems

The 5 carbonyl-based ligands from **Figure 8** saturated the Pb_4S_4 system as they were attached to each lead atom.

Table 7. IP of Pb_4S_4 – ligated systems

QD Ligated System	Calculated IP (eV)
Pb_4S_4 – Ligand 1	8.910 ± 0.044
Pb_4S_4 – Ligand 2	8.622 ± 0.007
Pb_4S_4 – Ligand 3	9.342 ± 0.007
Pb_4S_4 – Ligand 4	9.500 ± 0.0004
Pb_4S_4 – Ligand 5	8.396 ± 0.121

The IP of the bare Pb_4S_4 core was found to be 7.608 eV (). From the data provided in **Table 7** it can be concluded that the addition of the carbonyl-based ligands to the Pb_4S_4 system increases the IP of the quantum dot from its bare core IP. This trend is seen regardless of the size of the ligands, meaning that all of the ligated systems have a higher IP than that of the bare Pb_4S_4 core. Therefore, the addition of carbonyl-based ligands stabilizes the

Pb₄S₄ bare core. However, there is no trend seen with IP in the addition of a specific number of methylene groups to the ligands on the system.

5.4.2 IP of Ligands Alone

SSE-MO was performed on the five carbonyl-based ligands from **Figure 8** alone.

Table 8. IPs of the carbonyl-based ligands without the Pb₄S₄ quantum dot

Ligand	Chemical Formula	Ligands Alone Calculated IP (eV)
Ligand 1	O-CO-H	$13.075 \pm 7.641 \times 10^{-6}$
Ligand 2	O-CO-CH ₃	$12.383 \pm 5.000 \times 10^{-4}$
Ligand 3	O-CO-CH ₂ -CH ₃	$12.364 \pm 6.070 \times 10^{-5}$
Ligand 4	O-CO-CH ₂ -CH ₂ -CH ₃	$12.348 \pm 2.012 \times 10^{-5}$
Ligand 5	O-CO-CH ₂ -CH ₂ -CH ₂ -CH ₃	$12.202 \pm 2.000 \times 10^{-4}$

It was found that the IP of the ligands alone, those not attached to the Pb₄S₄ quantum dot, had a much higher IP than that of the ligated systems (**Table 7**). In addition, ligand 1 with no methyl (CH₃) or methylene (CH₂) groups attached, had a notably higher IP than the other ligands (**Error! Reference source not found.**). **Table 8** demonstrates that ligands 2 – 5 have similar IPs, with the average across the four ligands being 12.324 ± 0.083 eV. The low standard deviation of the average IP solidifies this conclusion. Therefore, the addition of -CH₂ groups have little impact on the IP of the ligands alone. However, the addition of the -CH₂ groups for the quantum dot-ligated systems with ligands 2 – 5 attached shows much more variation (**Table 7**). The average IP for the Pb₄S₄ ligated systems with ligands 2 – 5 is 8.965 ± 0.538 eV, which is a much higher standard deviation than that of the ligands alone. Therefore, it can be concluded that the addition of ligands to the

bare Pb₄S₄ core has a larger impact on IP than when the ligands are alone. In addition, the IPs presented in **Table 8** are much higher than that of the ligated systems. This demonstrates that the ligands on their own are extremely stable and non-reactive; however, when they are added to a Pb₄S₄ quantum dot this system becomes more reactive, but not as reactive as the bare core system.

5.4.3 Ligation Impact on Pb₄S₄

To wrap up the monodentate ligand calculations, the IP of the bare Pb₄S₄ cores was examined. These calculations were obtained by stripping the ligands off the bare core and performing SSE-MO on this bare system.

Table 9. Impact of ligation on Pb₄S₄ bare cores

QD Core	Pb ₄ S ₄ Core IP (eV)	PbS bond length(Å)
Pb ₄ S ₄ Bare Core	7.608 ± 0.028	3.690
Pb ₄ S ₄ – Ligand 1	5.337 ± 0.002	2.443 ± 0.031
Pb ₄ S ₄ – Ligand 2	4.707 ± 0.065	2.439 ± 0.039
Pb ₄ S ₄ – Ligand 3	6.412 ± 0.003	2.608 ± 0.207
Pb ₄ S ₄ – Ligand 4	5.774 ± 0.002	2.456 ± 0.046
Pb ₄ S ₄ – Ligand 5	6.318 ± 0.004	2.576 ± 0.157

It can be seen that attaching ligands to the Pb₄S₄ core has an impact on the geometry of the bare core. The PbS bond length for the ligated cores were much smaller than the non-ligated core, meaning the addition of ligands resulted in a more compact structure. In addition, the IP of the bare cores with no ligands were smaller than that of the geometry optimized bare Pb₄S₄ core, most likely due to the change in core geometry. Therefore, the Pb₄S₄ cores undergo a structural transformation with the bonding of the ligands, resulting a decrease in IP. The lower IP means that

the ligated cores are more reactive than the geometry optimized core. The attachment of ligands to Pb_4S_4 makes the bare core more reactive.

5.4.4 $\text{Pb}_{44}\text{S}_{44}$ - Ligated System

Table 10. Non-bridged calculated IPs for the $\text{Pb}_{44}\text{S}_{44}$ system

Number of Ligands	Calculated IP (eV)
0	6.958
1	7.584
2	7.593
3	7.586
4	7.568
5	7.576
6	7.569

This table demonstrates that the addition of ligands to the bare core increases the IP of the system, which was additionally seen with the Pb_4S_4 non-bridged ligated system in **Table 7**. Therefore, in these two systems attaching any number of carbonyl-based ligands stabilizes the bare core system. In this ligated $\text{Pb}_{44}\text{S}_{44}$ system the number of ligands attached did not have a large impact on the calculated SSE-MO IP as the average IP with one to six ligands attached is $7.579\text{eV} \pm 0.010$, which is an extremely small standard deviation.

5.5 Bridged Ligands

Up to six bridged ligands were attached to optimal lead atoms by the two oxygens from ligand 1 in $\text{Pb}_{44}\text{S}_{44}$.

Table 11. Bridged calculated IPs for the Pb₄₄S₄₄ system

Number of Ligands	Calculated IP (eV)
0	6.958
1	7.634
2	7.646
3	7.636
4	7.631
5	7.629
6	7.629

As shown in **Table 11** bridged ligands are stabilizing compared to the non-bridged or monodentate ligands (**Table 10**). This can be determined as the bridged ligands have a higher calculated IP as shown in **Figure 9**, meaning they are less reactive and more stable. The IP of the bare Pb₄₄S₄₄ core was found to be 6.960eV, **Error! Reference source not found..** Therefore, these results once again demonstrate that having ligands attached to the system, whether it is bridged or non-bridged, is stabilizing to the Pb₄₄S₄₄ system. It can additionally be seen that the number of bridged ligands added to the Pb₄₄S₄₄ system does not have a large impact on IP as the average IP is 7.634eV \pm 0.007, an extremely small standard deviation.

5.6 Chelating Ligands

Up to six ligand ones were added to the Pb₄₄S₄₄ system in the chelating configuration.

Table 12. Chelating ligands calculated IPs for the Pb₄₄S₄₄ system

Number of Ligands	Calculated IP (eV)
0	6.958
1	7.564
2	7.548
3	7.561
4	7.553
5	7.560
6	7.569

Table 12 once again shows that the addition of the chelating ligands increases the IP of the Pb₄₄S₄₄ system increases with the addition of ligands. Therefore, the addition of any type of ligand to Pb₄₄S₄₄ stabilizes the system. The number of chelating ligands added has little influence on the IP of the system as the average IP for one through 6 ligands attached to the system is 7.559eV \pm 0.008. Compared to the bridged and non-bridged systems this is the smallest standard deviation between the different ligand configurations.

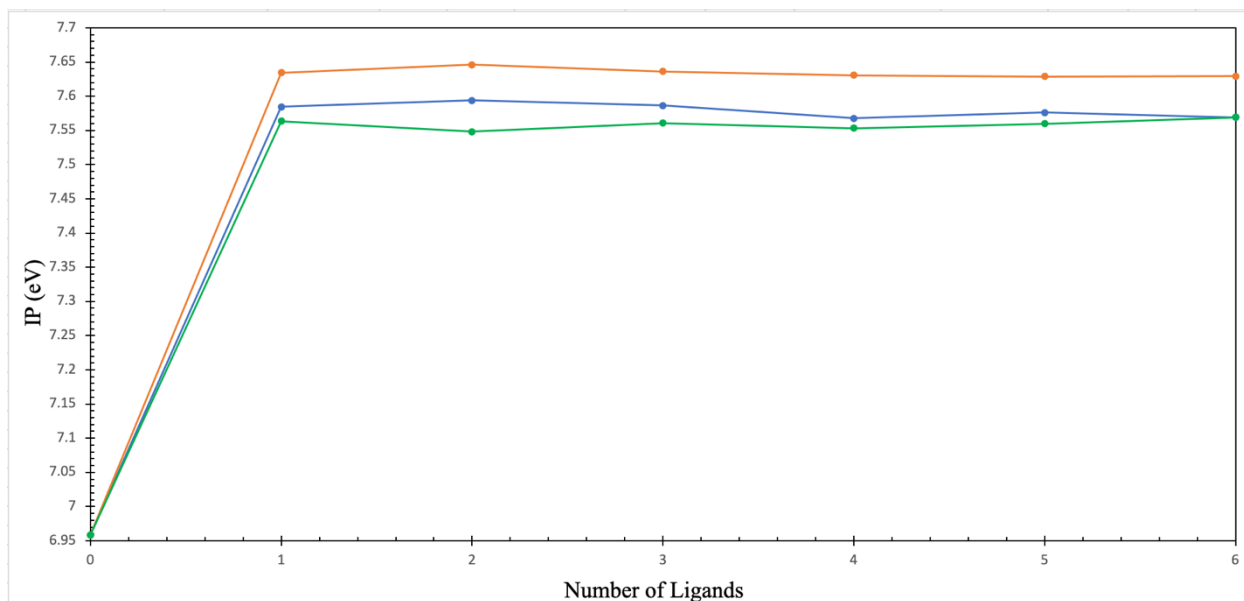


Figure 9. Demonstration of the IP relationship between the monodentate, bridged, and chelating ligands in the $\text{Pb}_{44}\text{S}_{44}$ system. The orange line on the top represents the bridged ligands, the blue, line in the middle signifies the non-bridged ligands, and the green bottom line is the chelating ligands.

Figure 9 shows the relationship between the IPs of the different ligand bonding patterns on the $\text{Pb}_{44}\text{S}_{44}$ system. The IPs of the bridged ligated systems are higher than those of the monodentate and chelating ligated systems, meaning this bonding pattern is the most stabilizing. This can be shown as the average IP with the ligands attached for the bridged ligated system was found to be $7.634\text{eV} \pm 0.006$ compared to $7.559\text{eV} \pm 0.008$ for the chelated system and $7.579\text{eV} \pm 0.010$ for the non-bridged ligands, but there is not a significant difference in the average IPs. The chemical intuition behind the bridged bonding pattern being the most stable is that in this configuration both oxygens in the ligand are attached to lead atoms, which forms a large, stable, open ring containing two lead atoms from the quantum dot system.

The IPs of the chelating system were the lowest, meaning this ligand configuration is the least stabilizing. This effect is most likely due to the tight four membered ring that is formed with the

chelating bonding pattern as only one lead atom is involved. The steric strain produced from this ring would be the least stabilizing out of the three bonding patterns. The monodentate bonding pattern is a standard chemical bonding pattern, which is most likely it produces average IPs in the middle of the other two bonding patterns. From this data it can also be seen that the number of ligands attached for each bonding configuration does not have a significant impact on IP.

Overall, understanding the IPs associated with the three ligand configurations allows for the IP of a ligated system to be used as a diagnostic tool to determine the bonding pattern on system surfaces.

5.7 Future directions

This work can serve as the foundation for several future studies. To begin, the bare core calculations can be performed on other size lead sulfide quantum dot systems to see if a trend in IP can be reached as the size of the system changes. However, the limiting factor for systems larger than those utilized in this work has been successfully running the Hartree-Fock calculations. Therefore, before further advancing in this direction the Hartree-Fock aspect of the calculation method must be improved.

In addition, the same monodentate ligand calculations can be performed on other lead sulfide systems, such as $\text{Pb}_{28}\text{S}_{28}$ and $\text{Pb}_{140}\text{S}_{140}$. These results can be analyzed to determine if the same behavior as demonstrated in the Pb_4S_4 and $\text{Pb}_{44}\text{S}_{44}$ ligated systems is seen. A limiting factor in this aspect of the work is that when increasing the size of the quantum dot challenges, the surface area increases as the square of the radius of the quantum dot. Therefore, more ligands can be attached to the systems, but completely saturating the lead atoms is computationally impractical due to the

time cost. This is why there were only six ligands used with $\text{Pb}_{44}\text{S}_{44}$. Therefore, when attaching the ligands to larger systems a similar method must be utilized. In addition, more than six ligands could be added to these larger systems to see if the IP remains consistent no matter how many ligands are present. These monodentate calculations on $\text{Pb}_{44}\text{S}_{44}$ could also be ran with the other carbonyl-based ligands (ligands 2-5) in the same configurations as the results presented in this work. Overall, in order to obtain well-rounded data, the IP of numerous configurations with the same ligands attached should be calculated and the results compared. This will allow for well-rounded, accurate data to be obtained and analyzed.

Furthermore, the same monodentate calculations on Pb_4S_4 can be run without all of the lead atoms saturated utilizing the same ligands to determine if the same trends are seen. This means attaching one, two, or three ligands to different lead atoms and comparing the results with the fully saturated Pb_4S_4 atom. In addition, these calculations can be run with different types of ligands, such as sulfur to nitrogen-based ligands, to see if this effects the IP trend produced.

Finally, the bridged and chelating ligand calculations can be performed on the same $\text{Pb}_{44}\text{S}_{44}$ system, but different configurations can be tested to determine if the same trends are seen. These configurations can also be tested with the other carbonyl-based ligands utilized in this work to determine if the number of methylene groups has an impact on this calculated IP. In addition, the ligand configurations used in this work can be tested on different size lead sulfide quantum dot systems. The results can be compared with those obtained in this study to test its widespread applicability.

6. Conclusion

This project determined the effect that the size of different lead sulfide quantum dots had on IP using the SSE-MO method. It was concluded that as the size of the quantum dot increases, the IP generally decreases. In addition, the effects of different sizes and types of carbonyl-based ligands on IP were demonstrated. When ligands were added to the bare Pb_4S_4 core, the IP of the system increased. It was also seen that the ligands alone have a higher IP than when they are attached to the bare lead sulfide core. When analyzing the ligated Pb_4S_4 system IPs it can be determined that the CH_2 groups of the carbonyl-based ligands do not have a large impact on the ligands when they are alone, but they have a notable impact on the overall IP of the Pb_4S_4 system. The addition of these ligands changed the geometry of the Pb_4S_4 bare cores, making them more compact, which caused an overall decrease in the IP of the systems. Therefore, the addition of ligands to Pb_4S_4 makes their bare core more reactive.

The addition of bridged, monodentate, and chelating ligands to the $\text{Pb}_{44}\text{S}_{44}$ system increased its overall IP. This means that the addition of any form of carbonyl-based ligand stabilizes this system. This was seen with both $\text{Pb}_{44}\text{S}_{44}$ and Pb_4S_4 when monodentate ligands were added, meaning that the addition of ligands stabilizes the lead sulfide system. The bridged ligands, where both oxygens from the ligand were attached to separate lead atoms, had a higher IP than that of the non-bridged and chelating ligands. This means that the addition of bridged ligands is more stabilizing than the addition of monodentate and chelating ligand bonding patterns. The calculated IP for the chelating ligand systems was the lowest, meaning this configuration is the least stabilizing.

The addition of any form of carbonyl-based ligands to Pb_4S_4 and $\text{Pb}_{44}\text{S}_{44}$ stabilizes the systems. From this work, it is shown that IP can be used as an experimental technique to determine the bonding pattern on system surfaces and as a method to help predict the materials and conditions necessary for nanomaterial manufacturing.

7. References

- (1) Hickey, W. *Where People Go To Check The Weather*. FiveThirtyEight. <https://fivethirtyeight.com/features/weather-forecast-news-app-habits/> (accessed 2022-09-26).
- (2) *6 tools our meteorologists use to forecast the weather*. <https://www.noaa.gov/stories/6-tools-our-meteorologists-use-to-forecast-weather> (accessed 2022-09-26).
- (3) *What are Ligands?*. News-Medical.net. <https://www.news-medical.net/life-sciences/Ligands-An-Overview.aspx> (accessed 2022-09-27).
- (4) Spanedda, N.; McLaughlin, P. F.; Beyer, J. J.; Chakraborty, A. Investigation of Ionization Potential in Quantum Dots Using the Stratified Stochastic Enumeration of Molecular Orbitals Method. *J. Chem. Theory Comput.* **2022**. <https://doi.org/10.1021/acs.jctc.2c00329>.
- (5) *What are quantum dots?* https://www.nanowerk.com/what_are_quantum_dots.php (accessed 2022-09-26).
- (6) Ahamed, M. I.; Ahamed, M.; Muthaiyan, R. Modelling of Density of States and Energy Level of Chalcogenide Quantum Dots. *International Review of Applied Sciences and Engineering* **2021**, 13 (1), 42–46. <https://doi.org/10.1556/1848.2021.00288>.
- (7) Jayawardhana, M and GAMALATH, K.A.I.L. Electronic Structures of CdSe Quantum Dots Embedded in ZnSe. *World Scientific News* **2017**, 86, 205–225.
- (8) *De Broglie thermal wavelength*. Chemistry LibreTexts. [https://chem.libretexts.org/Bookshelves/Physical_and_Theoretical_Chemistry_Textbook_Maps/Supplemental_Modules_\(Physical_and_Theoretical_Chemistry\)/Fundamentals/De_Broglie_thermal_wavelength](https://chem.libretexts.org/Bookshelves/Physical_and_Theoretical_Chemistry_Textbook_Maps/Supplemental_Modules_(Physical_and_Theoretical_Chemistry)/Fundamentals/De_Broglie_thermal_wavelength) (accessed 2022-11-10).

- (9) Nirmal, M.; Brus, L. Luminescence Photophysics in Semiconductor Nanocrystals. *Acc. Chem. Res.* **1999**, 32 (5), 407–414. <https://doi.org/10.1021/ar9700320>.
- (10) Zhao, Y.; Burda, C. Development of Plasmonic Semiconductor Nanomaterials with Copper Chalcogenides for a Future with Sustainable Energy Materials. *Energy Environ. Sci.* **2012**, 5 (2), 5564–5576. <https://doi.org/10.1039/C1EE02734D>.
- (11) Sargent, E. H. Colloidal Quantum Dot Solar Cells. *Nature Photon* **2012**, 6 (3), 133–135. <https://doi.org/10.1038/nphoton.2012.33>.
- (12) Cotta, M. A. Quantum Dots and Their Applications: What Lies Ahead? *ACS Appl. Nano Mater.* **2020**, 3 (6), 4920–4924. <https://doi.org/10.1021/acsanm.0c01386>.
- (13) Bederak, D.; Dirin, D. N.; Sukharevska, N.; Momand, J.; Kovalenko, M. V.; Loi, M. A. S-Rich PbS Quantum Dots: A Promising p-Type Material for Optoelectronic Devices. *Chem. Mater.* **2021**, 33 (1), 320–326. <https://doi.org/10.1021/acs.chemmater.0c03865>.
- (14) *Principle of Optical Emission Spectrometry*. <https://www.shimadzu.com/an/products/elemental-analysis/oes-app/principle-of-optical-emission-spectrometry/index.html> (accessed 2022-11-11).
- (15) Zamberlan, F.; Turyanska, L.; Patanè, A.; Liu, Z.; L. Williams, H. E.; W. Fay, M.; A. Clarke, P.; Imamura, Y.; Jin, T.; D. Bradshaw, T.; R. Thomas, N.; M. Grabowska, A. Stable DHLA–PEG Capped PbS Quantum Dots: From Synthesis to near-Infrared Biomedical Imaging. *Journal of Materials Chemistry B* **2018**, 6 (4), 550–555. <https://doi.org/10.1039/C7TB02912H>.
- (16) Wagner, A. M.; Knipe, J. M.; Orive, G.; Peppas, N. A. Quantum Dots in Biomedical Applications. *Acta Biomaterialia* **2019**, 94, 44–63. <https://doi.org/10.1016/j.actbio.2019.05.022>.

- (17) Walling, M. A.; Novak, J. A.; Shepard, J. R. E. Quantum Dots for Live Cell and In Vivo Imaging. *International Journal of Molecular Sciences* **2009**, *10* (2), 441–491. <https://doi.org/10.3390/ijms10020441>.
- (18) Li, Z.; Zhao, X.; Huang, C.; Gong, X. Recent Advances in Green Fabrication of Luminescent Solar Concentrators Using Nontoxic Quantum Dots as Fluorophores. *Journal of Materials Chemistry C* **2019**, *7* (40), 12373–12387. <https://doi.org/10.1039/C9TC03520F>.
- (19) Hyun, B.-R.; Zhong, Y.-Wu.; Bartnik, A. C.; Sun, L.; Abruña, H. D.; Wise, F. W.; Goodreau, J. D.; Matthews, J. R.; Leslie, T. M.; Borrelli, N. F. Electron Injection from Colloidal PbS Quantum Dots into Titanium Dioxide Nanoparticles. *ACS Nano* **2008**, *2* (11), 2206–2212. <https://doi.org/10.1021/nn800336b>.
- (20) *Electron Affinity*. Chemistry LibreTexts. [https://chem.libretexts.org/Bookshelves/Physical_and_Theoretical_Chemistry_Textbook_Maps/Supplemental_Modules_\(Physical_and_Theoretical_Chemistry\)/Physical_Properties_of_Matter/Atomic_and_Molecular_Properties/Electron_Affinity](https://chem.libretexts.org/Bookshelves/Physical_and_Theoretical_Chemistry_Textbook_Maps/Supplemental_Modules_(Physical_and_Theoretical_Chemistry)/Physical_Properties_of_Matter/Atomic_and_Molecular_Properties/Electron_Affinity) (accessed 2022-10-11).
- (21) *Peak External Photocurrent Quantum Efficiency Exceeding 100% via MEG in a Quantum Dot Solar Cell* | *Science*. <https://www.science.org/doi/10.1126/science.1209845> (accessed 2022-09-26).
- (22) Malyarevich, A. M.; Savitski, V. G.; Prokoshin, P. V.; Posnov, N. N.; Yumashev, K. V.; Raaben, E.; Zhilin, A. A. Glass Doped with PbS Quantum Dots as a Saturable Absorber for 1-Mm Neodymium Lasers. *J. Opt. Soc. Am. B, JOSAB* **2002**, *19* (1), 28–32. <https://doi.org/10.1364/JOSAB.19.000028>.

- (23) Ankah, G. N.; Büchele, P.; Poulsen, K.; Rauch, T.; Tedde, S. F.; Gimmmler, C.; Schmidt, O.; Kraus, T. PbS Quantum Dot Based Hybrid-Organic Photodetectors for X-Ray Sensing. *Organic Electronics* **2016**, *33*, 201–206. <https://doi.org/10.1016/j.orgel.2016.03.023>.
- (24) *What Is Ionization Energy?*. ThoughtCo. <https://www.thoughtco.com/ionization-energy-and-trend-604538> (accessed 2022-09-26).
- (25) Phillips, H.; Zheng, Z.; Geva, E.; Dunietz, B. D. Orbital Gap Predictions for Rational Design of Organic Photovoltaic Materials. *Organic Electronics* **2014**, *15* (7), 1509–1520. <https://doi.org/10.1016/j.orgel.2014.03.040>.
- (26) *Fragmentation Patterns in Mass Spectra*. Chemistry LibreTexts. [https://chem.libretexts.org/Bookshelves/Analytical_Chemistry/Supplemental_Modules_\(Analytical_Chemistry\)/Instrumental_Analysis/Mass_Spectrometry/Fragmentation_Patterns_in_Mass_Spectra](https://chem.libretexts.org/Bookshelves/Analytical_Chemistry/Supplemental_Modules_(Analytical_Chemistry)/Instrumental_Analysis/Mass_Spectrometry/Fragmentation_Patterns_in_Mass_Spectra) (accessed 2022-09-27).
- (27) Machon, D.; Pischedda, V.; Le Floch, S.; San-Miguel, A. Perspective: High Pressure Transformations in Nanomaterials and Opportunities in Material Design. *Journal of Applied Physics* **2018**, *124* (16), 160902. <https://doi.org/10.1063/1.5045563>.
- (28) *Perspective: High pressure transformations in nanomaterials and opportunities in material design: Journal of Applied Physics: Vol 124, No 16*. <https://aip.scitation.org/doi/10.1063/1.5045563> (accessed 2022-09-26).
- (29) Teunis, M. B.; Dolai, S.; Sardar, R. Effects of Surface-Passivating Ligands and Ultrasmall CdSe Nanocrystal Size on the Delocalization of Exciton Confinement. *Langmuir* **2014**, *30* (26), 7851–7858. <https://doi.org/10.1021/la501533t>.

- (30) Kennehan, E. R.; Munson, K. T.; Doucette, G. S.; Marshall, A. R.; Beard, M. C.; Asbury, J. B. Dynamic Ligand Surface Chemistry of Excited PbS Quantum Dots. *J. Phys. Chem. Lett.* **2020**, *11* (6), 2291–2297. <https://doi.org/10.1021/acs.jpcllett.0c00539>.
- (31) Wright, J. *Introduction To Bridging Ligands - Metal Complexes*. Texas Powerful Smart. <https://www.texaspowerfulsmart.com/metal-complexes/introduction-to-bridging-ligands.html> (accessed 2022-11-10).
- (32) 3.1.1: *Chelating Ligands*. Chemistry LibreTexts. [https://chem.libretexts.org/Courses/Saint_Marys_College_Notre_Dame_IN/CHEM_342%3A_Bio-inorganic_Chemistry/Readings/Week_3%3A_Metal-Ligand_Interactions_continued.../3.1_Ligands_with_more_than_one_donor_atom_\(Chelating_Ligands\)_have_enhanced_metal_ion_affinity/3.1.1%3A_Chelating_Ligands](https://chem.libretexts.org/Courses/Saint_Marys_College_Notre_Dame_IN/CHEM_342%3A_Bio-inorganic_Chemistry/Readings/Week_3%3A_Metal-Ligand_Interactions_continued.../3.1_Ligands_with_more_than_one_donor_atom_(Chelating_Ligands)_have_enhanced_metal_ion_affinity/3.1.1%3A_Chelating_Ligands) (accessed 2022-09-26).
- (33) Donald A. McQuarrie; John D. Simon. *Physical Chemistry A Molecular Approach*, 1st Edition.; University Science Books, 1997.
- (34) Sherrill, C. D. An Introduction to Hartree-Fock Molecular Orbital Theory. 8.
- (35) Elward, J. M.; Irudayanathan, F. J.; Nangia, S.; Chakraborty, A. Optical Signature of Formation of Protein Corona in the Firefly Luciferase-CdSe Quantum Dot Complex. *J. Chem. Theory Comput.* **2014**, *10* (12), 5224–5228. <https://doi.org/10.1021/ct500681m>.
- (36) Lin, H.; Truhlar, D. G. QM/MM: What Have We Learned, Where Are We, and Where Do We Go from Here? *Theor Chem Acc* **2007**, *117* (2), 185. <https://doi.org/10.1007/s00214-006-0143-z>.

- (37) William H. Press; Saul A. Teukolsky; William T. Vetterling; Brian P. Flannery. *Numerical Recipes in Fortran 77*, Second Edition.; Press Syndicate of the University of Cambridge, 1986.